Journal of Coastal Research	15	4	892–901	Royal Palm Beach, Florida	Fall 1999

Generation of Nearshore Bars by Multi-Domain Hybrid Numerical Model

C.E. Lee, M.H. Kim and B.L. Edge

Department of Civil Engineering
Texas A&M University
College Station, TX 77843, USA

ABSTRACT

LEE, C.E.; KIM, M.H., and EDGE, B.L., 1999. Generation of Nearshore Bars by Multi-Domain Hybrid Numerical Model. *Journal of Coastal Research,* 15(4), 892–901. Royal Palm Beach (Florida), ISSN 0749-0208.

A multi-domain hybrid numerical model for the prediction of cross-shore sediment transport including bar generation and movement is developed in this paper based on the macro-scale sediment transport rate and conservation equations. The surf zone is divided into several sub-domains, such as numerical post-breaking zone and analytical breaking and pre-breaking zones. Different empirical sediment transport rate equations are defined in each region. In the post-breaking zone, an inhomogeneous diffusion equation is solved with moving boundary conditions. The solutions in each domain are matched at the patching boundaries by the continuity of the beach profile and sediment transport rate. It is verified that the present hybrid numerical model reasonably simulates beach erosion, dune recession, and bar formation and movement. The model conserves the overall sediment volume and converges toward a steady-state solution. The model is also validated through comparison with laboratory and field data. The numerical model can straight-forwardly be extended to generate multiple bars. Using the developed program, it is shown that the bar formation can be greatly influenced by the pattern of the storm surge hydrograph.

ADDITIONAL INDEX WORDS: *Beach profile change, cross shore sediment transport, dune recession.*

INTRODUCTION

The quantitative prediction of beach profile change is of great importance in various coastal engineering projects. In particular, it is essential for effective beach nourishment, identifying susceptible areas to coastal hazards, and establishing coastal setback lines. Despite the importance of the problem, the details of the sediment transport processes caused by the change of surf-zone environment are not well understood.

Until now, three different approaches have been used to quantitatively predict cross-shore sediment transport in the surf zone. The first is based on the simple equilibrium profile concept developed through extensive field observations (BRUUN, 1954; DEAN, 1977; 1991). The second is the process-based approach where attempt was made to analyze the details of the local flow and sediment movement patterns inside the surf zone (ROELVINK and BROKER, 1993). This method is theoretically more rigorous and can include some possibly important local features. However, the result may not be reliable if the detailed hydrodynamics inside the surf zone cannot be accurately calculated (NAIRN, 1991; WISE *et al.,* 1991). The third approach is based on the empirically-determined macro-scale sediment transport rate equation used with sediment volume conservation. KRIEBEL and DEAN (1985), KOBAYASHI (1987), LARSON and KRAUS (1989), NISHI and SATO (1994), and LEE *et al.* (1996) used this macro-scale approach and showed that this method can reasonably simulate the beach profile change for a given storm condition. In particular, LEE *et al.* (1996) used an inhomogeneous diffusion equation with moving boundary conditions and developed relevant finite-difference schemes. The numerical results including beach erosion, dune recession, and offshore deposition compared favorably with experimental and field data. The bar generation, however, was not studied in LEE *et al.* (1996). In the present paper, a multi-domain hybrid numerical model is employed to add bar-generation features to the beach-erosion program developed in LEE *et al.* (1996).

The bar generation is one of the most important features associated with the beach evolution prediction in the surf zone. Bars tend to reduce erosive energy entering the surf-zone by breaking the higher incident waves. A bar is formed by the sediment transported from neighboring areas and several bars may appear along a beach profile, often having a distinct trough on the shoreward side. In many cases, a prominent bar is located near the breaking point (KEULEGAN, 1948) and smaller inner bars are also frequently observed. During storms, bars are formed by the sediment moved from the beach face, whereas under lower waves, bars tend to lose volume and move onshore to resupply the surf zone and beach. In this paper, in addition to the beach erosion and dune recession, the formation and movement of nearshore bars by a given storm-surge hydrograph is numerically studied.

Several mechanisms (*e.g.* DAVIDSON-ARNOTT, 1981; DALLY and DEAN, 1984; BOCZAR-KARAKIEWICZ *et al.,* 1995) have been proposed for formation of offshore bars. Among them, wave breaking is considered to be the primary cause (DEAN

98008 received 3 January 1998; accepted in revision 17 December 1998.

et al., 1992) and the scope of this paper is limited to bar generation by breaking waves. VAN HIJUM (1975, 1977), KAJIMA *et al.* (1982) and LARSON and KRAUS (1989) have suggested various empirical equations for the sediment transport rate including bars based on large scale experiments. Numerous field studies (*e.g.* LARSON and KRAUS, 1994; LIPPMANN and HOLMAN, 1990; SALLENGER *et al.,* 1985) have also been conducted to better understand the formation of nearshore bars. However, there are so many parameters and uncertainties involved that there exist no universally-valid theoretical or empirical models to cover such an extensive data set. LARSON and KRAUS (1989), and LARSON *et al.* (1990) developed a macro-scale numerical model called SBEACH to simulate beach erosion and bar formation in the surf zone. Their numerical model in the post-breaking zone is based on the modified KRIEBEL and DEAN (1985) sediment-transport-rate equation. They also introduced two sub-domains called breaker transition zone and pre-breaking zone and assumed that the sediment transport rates in those regions can be described by exponential functions. Their numerical results compared favorably with large-scale experimental results.

In the present paper, we have developed a multi-domain hybrid numerical model for the prediction of cross-shore sediment transport including dune recession, and the generation and movement of nearshore bars. The beach erosion and dune recession are treated similar to LEE *et al.* (1996). Two subdomains are additionally introduced near the breaking point and empirically-based explicit transport rate equations are used to generate bars. In the breaker transition (or breaking) zone, a Gaussian distribution of sediment transport rate was used, as suggested by KAJIMA *et al.* (1982), in view of that the peak sediment transport does not necessarily occur at the plunging point (KAJIMA *et al.,* 1982; KEULEGAN, 1948). The beach profiles and sediment transport rates in each region are then matched at all the boundaries. The developed program is efficient and robust and converges toward a steady state solution.

The present numerical model was also validated through comparison with large-scale experimental data and field measurement. The present method can straightforwardly be extended to multi-bar problems by systematically adding more subdomains, as explained in the Appendix. The theoretical basis and numerical treatment of this hybrid method are explained in the next section and various numerical results and relevant discussion are presented in the following section.

THEORY AND NUMERICAL MODEL

In this section, we consider the governing equation, sediment transport rate equation, and related boundary conditions for beach erosion and bar generation. It is assumed that the beach consists of homogeneous sediment and the variation of water level inside the surf zone with time is known. In the present analysis, the long-shore sediment transport is not considered implying uniform transport alongshore. Thus, the model is not applicable near coastal structures or longshore discontinuities in bathymetry. As shown in Figure 1, the whole computational domain is divided into three subdomains, including post-breaking zone, breaking zone, and pre-breaking zone. In each region, different sediment transport rate equations are used.

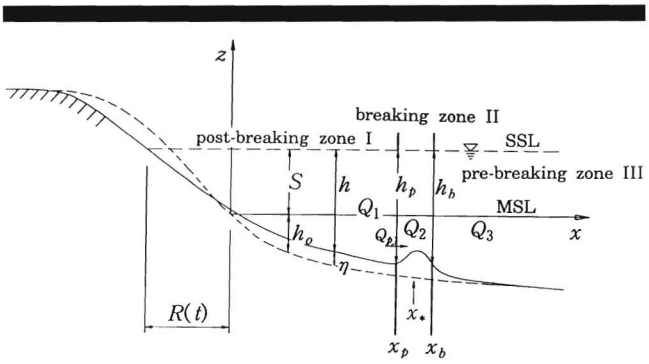

Figure 1. Coordinate system and definition of geometric variables.

The continuity equation for bottom sediment in each zone is expressed as

$$\frac{\partial \eta}{\partial t} = -\frac{\partial Q}{\partial x}, \qquad -R(t) \le x \le \infty \tag{1}$$

in which the vertical beach displacement $\eta(x, t) = h_o(x) + S(x, t) - h(x, t)$ with h_o, S and h being the initial profile, water level, and instantaneous local water depth, respectively. The symbol Q is the time-averaged net cross-shore volumetric sediment transport rate per unit alongshore width and x, t are spatial and temporal independent variables, respectively. $R(t)$ is the distance from the origin to the point $h(x, t) = 0$. The instantaneous water level S can in principle vary with time and space inside the surf zone. However, in this paper, the spatial variability of S is not considered and a constant hydrograph model is used. In reality, the height of broken waves in general decays as they propagate onshore but it is assumed that it is compensated by the wave and wind setup.

In the post-breaking zone, we use the following sediment transport rate equation which was suggested in KOBAYASHI (1987) and LEE *et al.* (1996):

$$Q_1 = D\frac{\partial h}{\partial x} - K, \qquad -R(t) \le x \le x_p(t) \tag{2}$$

in which empirical parameters D and K are related to the wave condition and sediment characteristics. The dune recession and offshore deposition rates in general increase with D but decrease with K. The range of D and K values and their influence on the erosion pattern are detailed in LEE *et al.* (1996). The symbol $x_p(t)$ is the distance from the origin to the point $h(x, t) = h_p(t)$ with h_p being the water depth at the plunging point. In both KOBAYASHI (1987) and LEE *et al.* (1996), the following formulas were suggested:

$$D = \alpha\sqrt{h_p} \tag{3}$$

$$K = \frac{2}{3}\alpha A^{3/2} \tag{4}$$

in which A and α are parameters related to the sediment size and fall velocity (DEAN, 1977; LEE *et al.,* 1996). The param-

Table 1. *Input data for the present hybrid numerical model.*

Case	Hannover	CE Case 300	CE Case 400
Wave height, H_o (m)	1.50	1.68	1.62
Wave period, T (sec)	6.0	11.3	5.6
Initial beach slope, S_o	1/4 & 1/20	1/15	1/15
Sand size, d_{50} (mm)	0.33	0.22	0.22
Breaking depth, h_b (m)	2.0	2.2	2.2
D (m²/sec)	0.012	0.013	0.013
K (m²/sec)	0.00054	0.00044	0.00044
λ_2 (1/m)	0.22	0.11	0.15
Run-up height, Z_r (m)	0.87	2.06	1.05

eter A is the constant used for equilibrium beach profile. The parameter α can be associated with Dean's parameter K (DEAN, 1977).

After combining (1), (2), (3), and (4), we obtain the following inhomogeneous diffusion equation for the instantaneous water depth h:

$$\frac{\partial h}{\partial t} = D\frac{\partial^2 h}{\partial x^2} + \frac{\partial S}{\partial t}, \qquad -R(t) \le x \le x_p(t). \tag{5}$$

In addition, the boundary conditions at the receding front and advancing plunging point are given by

$$Q_1 = -\eta\frac{dR}{dt}, \qquad x = -R(t) \tag{6}$$

$$Q_1 = Q_p + \eta\frac{dx_p}{dt}, \qquad x = x_p(t) \tag{7}$$

where Q_p is the sediment transport rate at the plunging point. The above equations mathematically describe the conservation of sediment flux at the moving boundaries. After substituting Eq. (2) into Eqs. (6) and (7), we obtain

$$D\frac{\partial h}{\partial x} = K - (h_o + S)\frac{dR}{dt}, \qquad x = -R(t) \tag{8}$$

$$D\frac{\partial h}{\partial x} = K + Q_p + (h_o + S - h_p)\frac{dx_p}{dt}, \qquad x = x_p(t). \tag{9}$$

The governing equation (5) can then be solved with the moving boundary conditions (8), (9) and an initial condition $h(x, o) = h_o(x) + S(x, o)$, as described in LEE *et al.* (1996).

The sediment transport rate equations in the breaking zone II and pre-breaking zone III are assumed to have the following explicit expressions

$$Q_2 = q_*(t)e^{-\lambda_1(x-x_*)^2}, \qquad x_p \le x \le x_b \tag{10}$$

$$Q_3 = q_b(t)e^{-\lambda_2(x-x_b)}, \qquad x_b \le x \le \infty \tag{11}$$

in which $x_b(t)$ is the breaking point set to be $x_b = x_p + 3H_b$ as suggested by LARSON and KRAUS (1989). H_b is the wave height at the breaking point. The breaker-depth index (breaker height to breaker depth ratio) is a function of wave height, wave length, and beach slope. A typical laboratory data (SMITH and KRAUS, 1991) shows considerable scatter to make it difficult to find a simple relationship among them. In this study, breaker-depth index = 0.78 is used for simplicity. The symbols $q_*(t)$ and $q_b(t)$ are time-dependent amplitude functions for the respective sediment transport rates in regions II and III. The equation (11) is established from the intuition that sediment transport rate attenuates exponentially from the breaking point. The equation (10) is different from the exponential function used in SBEACH and was guided by KEULEGAN's (1948) experimental result. The equation means that the sediment transport rate in domain II has Gaussian distribution (KAJIMA *et al.*, 1982) which is peaked at a point x_* positioned between plunging and breaking points. The spreading parameter λ_1 and decaying parameter λ_2 are related to the sediment and wave properties, which should be determined empirically. In order to reduce the degrees of freedom, we assumed the relationship $\lambda_1 = \gamma\lambda^n{}_2$ and conducted a parametric study to find appropriate γ and n values. Through this parametric study, the relationship $\lambda_1 = \lambda^2{}_2$ was established.

The requisite boundary condition at the junction of each domain is the continuity of the beach profile and sediment transport rate:

$$Q_1 = Q_2 + \eta\frac{dx_p}{dt}, \qquad h_1 = h_2 \quad \text{at} \quad h = h_p \tag{12}$$

$$Q_2 = Q_3, \qquad h_2 = h_3 \quad \text{at} \quad h = h_b. \tag{13}$$

Through the above matching boundary conditions, each domain is coupled with other domains.

So far, we described the governing equations and matching boundary conditions. The present numerical model is a "hybrid" model because the model is formed by the combination of numerical solutions (post-breaking zone I) and empirically based analytic solutions (breaking zone II, and pre-breaking zone III). We next explain the numerical implementation of the above equations and boundary conditions. The numerical treatment of the post-breaking zone I is close to that given in LEE *et al.* (1996).

An explicit forward-time and central-space finite difference scheme is used to solve the governing equation (5) in domain I:

$$h_j^{n+1} = \beta h_{j-1}^n + (1 - 2\beta)h_j^n + \beta h_{j+1}^n, \qquad -R(t) \le j\Delta x \le x_p(t) \tag{14}$$

in which $\beta = D\Delta t/(\Delta x)^2$, Δx is the spatial increment, and Δt the time increment. Similarly, the boundary conditions (8) and (9) can be expressed as

$$h_j^{n+1} = -\frac{2\beta\Delta x}{D}\left[K - (h_o + S)\frac{dR}{dt}\right] + (1 - 2\beta)h_j^n + 2\beta h_{j+1}^n, \qquad j\Delta x = -R(t) \tag{15}$$

$$h_j^{n+1} = \frac{2\beta\Delta x}{D}\left[K + Q_p - (h_o + S - h_p^n)\frac{dx_p}{dt}\right] + 2\beta h_{j-1}^n + (1 - 2\beta)h_j^n, \qquad j\Delta x = x_p(t). \tag{16}$$

After substituting the explicit sediment transport equations (10) and (11) into the continuity equation (1), we obtain

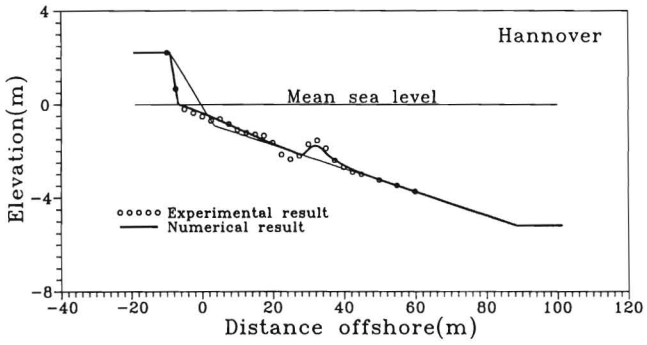

Figure 2. Comparison of the present numerical result with Hannover experimental data after 4.3 hours.

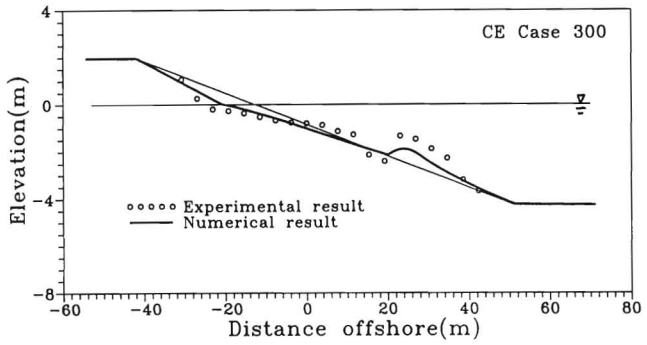

Figure 4. Comparison of the present numerical result with CE Case 300 experimental data after 5 hours.

$$h_2(x, t) = h_o(x) + S(x, t) - S(x, o) - \int_o^t 2\lambda_1 q_*(\tau)(x - x_*)e^{-\lambda_1(x-x_*)^2}\, d\tau, \quad x_p \le x \le x_b \tag{17}$$

$$h_3(x, t) = h_o(x) + S(x, t) - S(x, o) - \int_o^t \lambda_2 q_b(\tau)e^{-\lambda_2(x-x_b)}\, d\tau, \quad x_b \le x \le \infty \tag{18}$$

in which τ is a dummy variable. From (12), the sediment transport rate, Q_p, at the boundary point $x = x_p$ becomes

$$Q_p = Q_2|_{x=x_p} = q_*(t)e^{-\lambda_1(x_p-x_*)^2} \tag{19}$$

Another matching boundary condition at the point $x = x_p$ yields

$$\left\{(K + Q_p) + (h_o(x_p) + S - h(x_p)^n)\frac{dx_p}{dt}\right\}\frac{2\Delta x\beta}{D} + 2\beta h^n(x_p - \Delta x) + (1 - 2\beta)h^n(x_p) = h^n(x_p) - 2\Delta t\lambda_1(x_p - x_*)Q_p + S(x, t) - S(x, o) \tag{20}$$

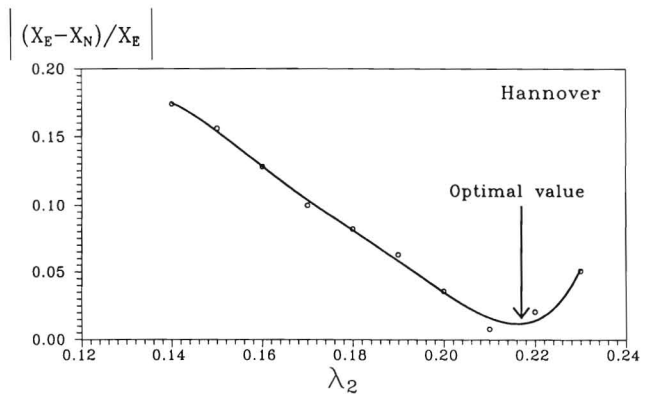

Figure 3. Optimal value of the parameter, λ_2.

Using the remaining matching boundary conditions given by Eq. (13), we obtain the following equations:

$$q_b(t) = q_*(t)e^{-\lambda_1(x_b-x_*)^2} \tag{21}$$

$$2q_*(t)\lambda_1(x_b - x_*)e^{-\lambda_1(x_b-x_*)^2} = \lambda_2 q_b(t) \tag{22}$$

From Eq. (21) and Eq. (22), we obtain

$$x_* = x_b - \frac{\lambda_2}{2\lambda_1} \tag{23}$$

Then, the remaining two unknowns $q_b(t)$ and $q_*(t)$ can be determined from (20) and (21).

In addition, the condition $x_p \le x_* \le x_b$ yields the following criterion for λ_1 and λ_2:

$$o \le \frac{\lambda_2}{2\lambda_1} \le x_b - x_p \tag{24}$$

Using $\lambda_1 = \lambda_2^2$ and $x_b - x_p = 3H_b$, we obtain the minimum values of λ_2

$$\lambda_2 \ge 0.167\frac{1}{H_b} \tag{25}$$

The boundary condition (15) can be used to determine the recession of the shoreline. The beach profile above storm

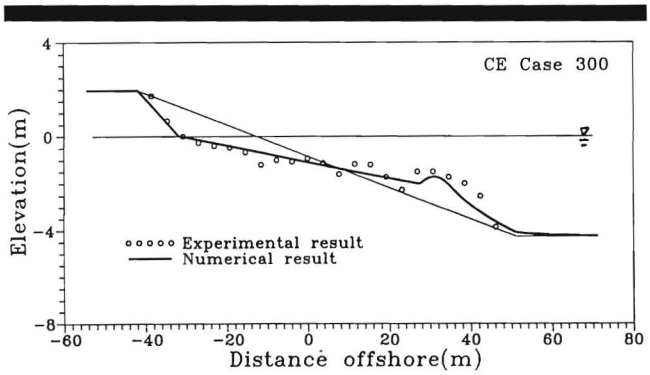

Figure 5. Comparison of the present numerical result with CE Case 300 experimental data after 50 hours.

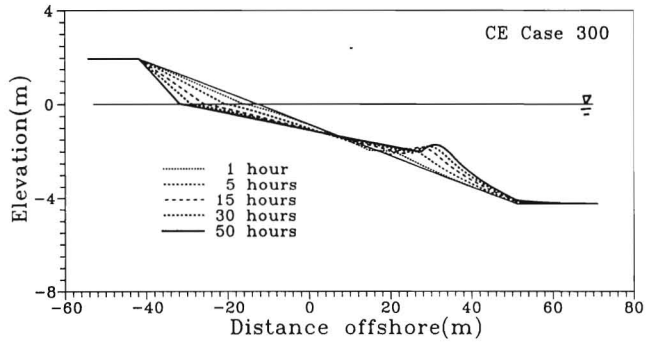

Figure 6. Time evolution of beach profile for the CE Case 300.

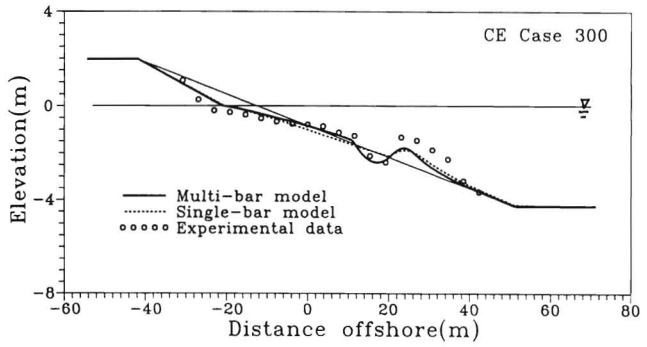

Figure 8. Comparison of the present single-bar and multi-bar numerical results with CE Case 300 experimental data after 5 hours.

surge level was then linearly extrapolated up to the point of maximum wave run-up which was computed from

$$Z_r = 1.47 H_o \left(\frac{\tan \beta}{\sqrt{H_o/L_o}} \right)^{0.79} \quad (26)$$

where H_o, L_o, and β are deepwater wave height, deepwater wavelength, and average slope of the beach front, respectively (LARSON and KRAUS, 1989). There were cases in which the recession of the shoreline proceeded beyond the run-up limit. In this case, the updated beach profile near the shoreline is linearly extrapolated to the dune crest.

RESULTS AND DISCUSSION

Numerical testing confirmed that the beach profile and sediment transport rate are continuous at each boundary, and the numerical model reasonably generates bars and converges toward a steady-state (or equilibrium) solution as time becomes large. The sediment volume is satisfactorily conserved in all the cases. The developed computer program was further validated through comparison with large-scale wave tank experiments and the field data of the Ocean City, Maryland, where a strong storm passed on January 2–5, 1992 (STAUBLE *et al.*, 1993). The selected experimental data are named as Hannover, CE Case 300, and CE Case 400, respectively. The Hannover data (DETTE and ULICZKA, 1987; SOUTHGATE, 1991) were obtained from the experiment conducted in the large wave tank at the University of Hannover, Germany in 1986, and the CE Case 300 and 400 data were obtained from the large-scale experiments conducted at the Coastal Engineering Research Center of U.S. Army Engr. Waterways Experiment Station (LARSON and KRAUS, 1989). The input data used in the present hybrid numerical model to compare with these experiments are summarized in Table 1.

In Figure 2, the numerically simulated beach profile after 4.3 hours is compared with the Hannover measurements. In this case, the initial profile has a steep foreshore slope connected to much gentler offshore slope, as shown in the figure. We can see that the bar generation as well as beach erosion and dune recession is reasonably predicted by the present

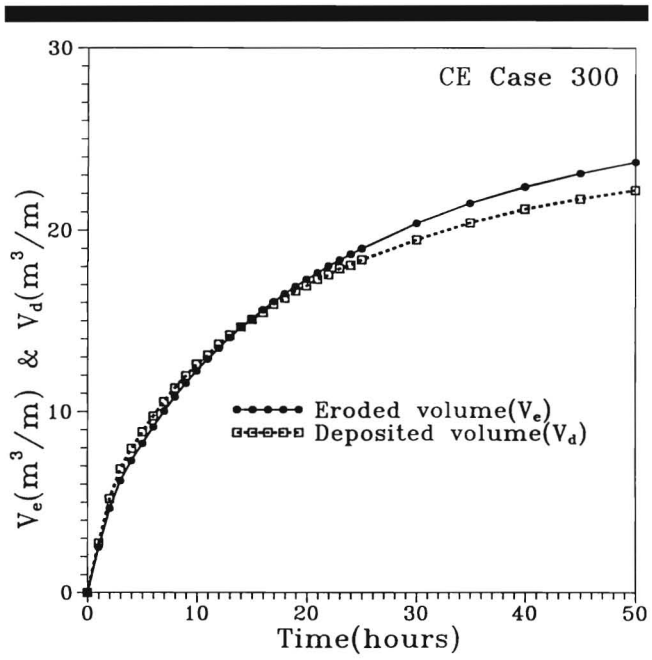

Figure 7. Eroded and deposited volumes as function of time for the CE Case 300.

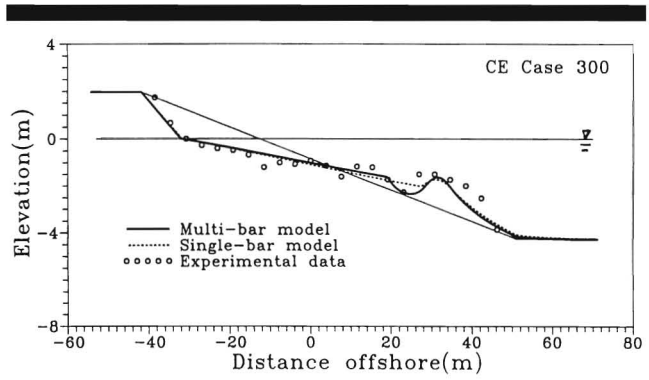

Figure 9. Comparison of the present single-bar and multi-bar numerical results with CE Case 300 experimental data after 50 hours.

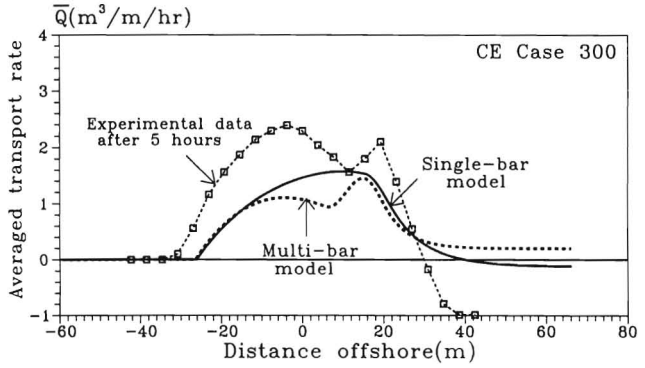

Figure 10. Comparison of the averaged net sediment transport rates computed from the single-bar and multi-bar numerical models with CE Case 300 experimental data after 5 hours.

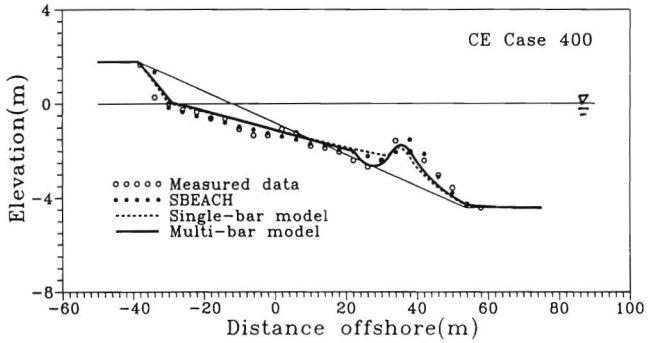

Figure 12. Comparison of the present single-bar and multi-bar numerical results with SBEACH and CE Case 400 experimental data after 40 hours.

numerical model except for the small-amplitude fluctuation between the shoreline and the prominent bar. These inner bars appear in many experimental results and are expected to be caused by multiple breakers. For this computation, we first determined the optimal value of the parameter λ_2, as shown in Figure 3, after comparing the computed bar position with the experimental data. In the figure, x_E and x_N are the experimental and numerical positions of bar crests, respectively.

We next compare the result of the present hybrid numerical model with CE Case 300 data. The parameter λ_2 was optimized in the same manner. Both numerical and measured beach profiles after 5 and 50 hours are plotted in Figures 4 and 5, respectively. The bar generation is slightly underpredicted by the numerical model, whereas good agreement is observed for the beach and dune areas except for the absence of small-amplitude inner bars in the calculation. These inner bars can in principle be numerically generated by introducing more subdomains, as explained in the Appendix. However, the detailed mechanism and features for multiple breakers and multiple bars are not well understood yet. We plot in Figure 6 the profile change of the same beach with time. At each time, we can clearly see that the eroded sediment from the dune and beach front is deposited near the bar. Also observed is the movement of the bar toward the offshore direction, which can also be confirmed from the physical model data. It can be seen that the speed of bar movement as well as the growth rate rapidly decays with time. Figure 7 shows the cumulative eroded and deposited sediment volumes with time. We can see that the overall sediment volume is reasonably conserved and each curve converges toward the steady state (or equilibrium condition) as time increases. Figures 8 and 9 show the results of the four-domain hybrid numerical model (see Appendix) that is used to generate an additional trough in front of the prominent bar. The overall correlation with laboratory data is improved, and a distinct bar trough is recovered after introducing an additional subdomain in front of the plunging point. By increasing the number of subdomains, we can numerically generate the inner bars as well. The next figure (Figure 10) shows the comparison of the measured average sediment transport rate with the computed values by the single- and multi-bar models. For this comparison, the following time-averaged sediment transport rate, $\bar{Q}$, was used.

$$\bar{Q}(x) = \frac{1}{t_2 - t_1} \int_{x_o}^{x} \{h_2(x, t_2) - h_1(x, t_1)\}\, dx \qquad (27)$$

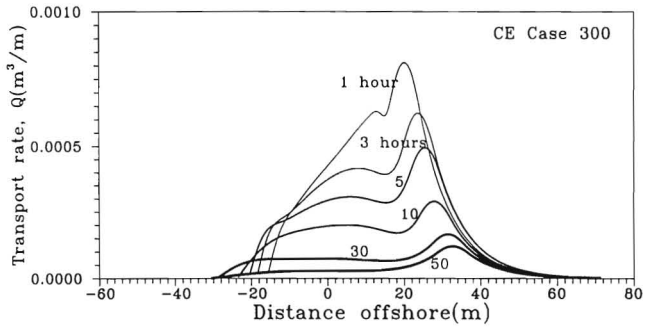

Figure 11. Computed net sediment transport rate as function of time for the CE Case 300.

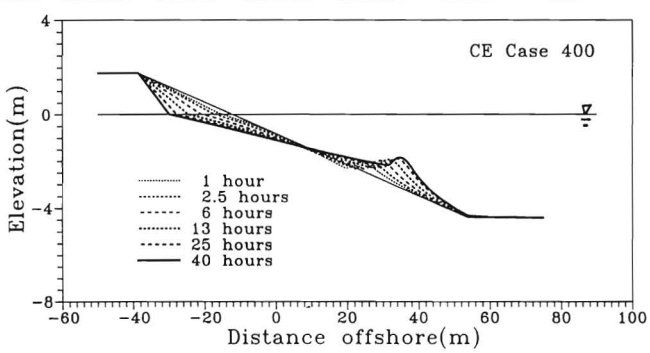

Figure 13. Time evolution of beach profile for the CE Case 400.

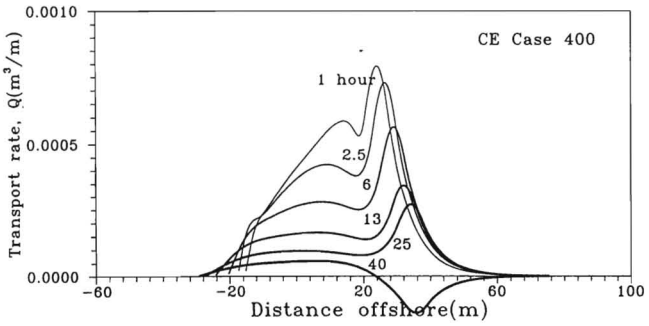

Figure 14. Net sediment transport rate as function of time for the CE Case 400.

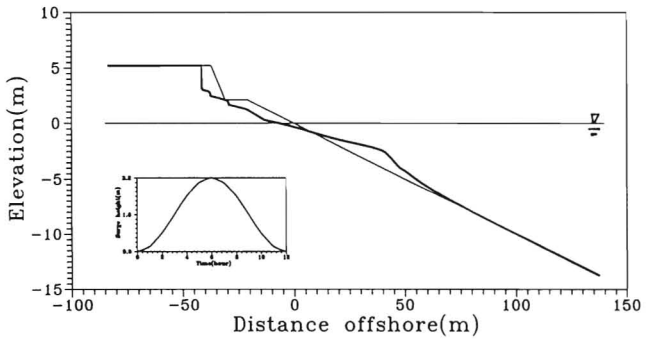

Figure 16. Beach profile change by a sine-shaped hydrograph.

in which t_1, t_2 are the times of profile surveys, and x_o is the reference point satisfying $\bar{Q}(x_o) = o$. As was already pointed out in the beach-profile comparison (Figures 4, 5, 8, and 9), the numerical values tend to underpredict the measured values. It is interesting that there are two peaks in the laboratory data, which can also be seen in the multi-bar (four-domain) numerical simulation. We next present in Figure 11 the instantaneous sediment transport rate calculated from the single-bar numerical model as function of shorenormal position as time progresses. The equations (2), (10) and (11) were used with Q_p to produce this result. The sediment transport rate is greatly reduced with time to reach a steady state. Also observed is the movement of the peak point toward the offshore direction, which causes bar movement. The general trend of our computation is similar to that observed in various physical model runs (*e.g.,* LARSON and KRAUS, 1989).

In the next figure (Figure 12), CE Case 400 is chosen to further validate our numerical result, which is also compared with the computation given in LARSON and KRAUS (1989). Both the present and SBEACH numerical models reasonably generate the nearshore bar after 40 hours, as shown in the figure. The four-domain numerical model better follows the measured beach profile than the three-domain model. In SBEACH, two exponential functions like (11) are used to represent the respective sediment transport rates in domain II and III, which implies that the peak sediment transport always occurs at the plunging point x_p. In contrast, Eq. (10) is more flexible in that the peak point is not necessarily the plunging point, which is also supported by KEULEGAN's (1948) experiment. Because the matching conditions at the patching boundaries are rigorously treated, the present numerical model does not exhibit any discontinuity in beach profile.

In the following numerical examples, only the single-bar numerical model is used unless otherwise mentioned. In Figure 13, the beach profile change with time is plotted for the CE 400 case. The overall trend is quite similar to that of Figure 6. The next figure (Figure 14) shows the corresponding instantaneous sediment transport rate as time progresses. The overall trend is analogous to that of Figure 11 except that negative (or onshore) sediment transport occurs near the bar after 40 hours. This kind of locally negative sediment transport near the breaking zone can also be observed in physical model tests (KAJIMA *et al.,* 1982). This kind of onshore sediment movement is expected to slow down continuous seaward movement of the bar to reach a steady state.

So far, our numerical examples have been limited to the case of constant wave condition. When water level (or wave condition) changes with time, the bar-generation mechanism is expected to be influenced by the movement of breaking and plunging points. Therefore, in the case of time-varying sea level, the bar formation is likely to be less conspicuous, as

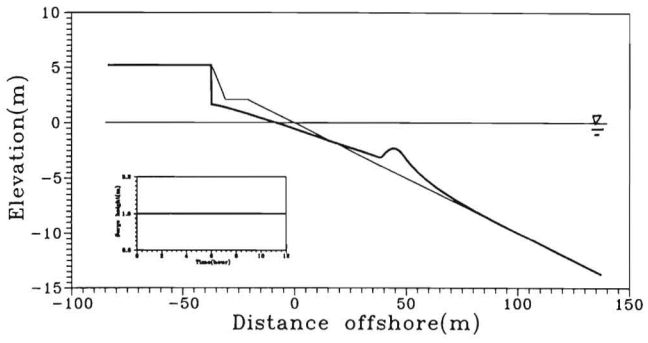

Figure 15. Beach profile change by a rectangular hydrograph.

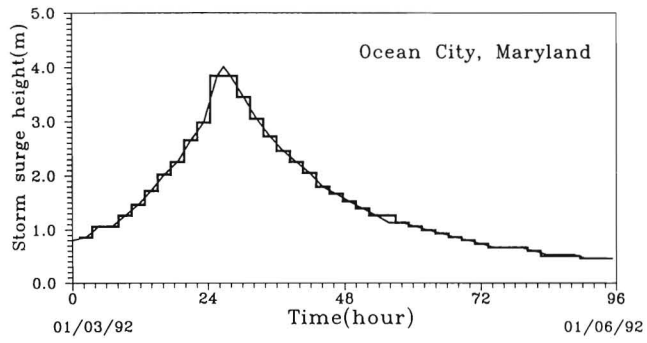

Figure 17. Storm surge hydrograph for the Ocean City, Maryland.

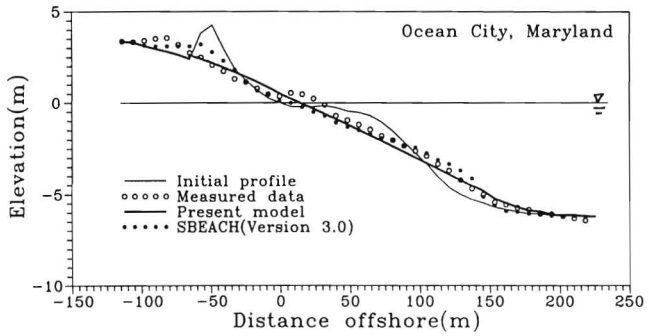

Figure 18. Comparison of the present post-storm profile with SBEACH and the measurements from 63rd street.

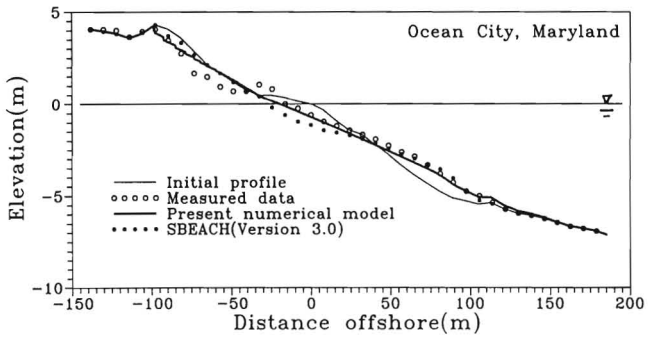

Figure 20. Comparison of the present post-storm profile with SBEACH and the measurements from 124th street.

has been reported by several researchers. In order to see this more clearly, we examined in Figures 15 and 16 the profile change of a particular beach after a 12-hour rectangular hydrograph and sinusoidally time-varying hydrograph. The heights of the initial dune and berm above MSL are 5.2 and 2.1 m, and the respective slopes are 0.5 and 0.1. The berm width is 10 m, $K = 0.00043$ m²/sec, $D = 0.019$ m²/sec, $\lambda_2 = 0.092$ 1/m, $\beta = 0.45$, and $\Delta x = 0.3$ m. The breaking point varies with time according to the change of sea level and beach profile. Interestingly, a distinct bar is formed when the water level remains constant, while it is hardly seen in the case of time-varying storm surge. Also observed is larger dune recession in the case of time-varying hydrograph. From this result, it is expected that nearshore bars tend to be less noticeable when the sea conditions change with time.

We next compare the result of the present hybrid numerical model with the field data collected in Ocean City, Maryland, in 1992. Seven survey lines were located from the southern end (37th street) to the northern end (124th street). The pre- and post-storm profiles of each line were measured two-months before and one-week after the storm surge. The time-dependent surge heights were measured during the four-day storm period, and the resulting hydrograph is shown in Figure 17. For illustration, we selected two lines, 63rd and 124th streets, where the longshore sediment transport was found to be minimal. We compared, in Figs. 18 and 20, the present numerical results with the field data. For this comparison, the median grain size of the beach is 0.35 mm, $K = 0.00058$ m²/sec, $D = 0.017$ m²/sec, $\lambda_2 = 0.045$ 1/m, $\beta = 0.45$, and $\Delta x = 0.3$ m. The initial and post-storm beach profiles at 63rd street are shown in Figure 18. The result of SBEACH (Version 3.0) calculated by ZHENG and DEAN (1995) is also presented. As discussed in the preceding example (Figures 15 and 16), no prominent bar is generated near the breaking zone, which is presumably due to the time-varying hydrograph. The time evolution of the same beach is presented in Figure 19. When the water level increases, severe erosion of dune and berm occurs. After the peak water level, we see little change in beach profile except for small amount of deposition in the offshore region.

Similar comparison between measured and computed results is also shown in Figure 20 for the 124th street line. The initial profile in this case is quite different from that of Figure 18; still, both the present and SBEACH numerical results correlate well with the field data. Again, no apparent bar is generated near the breaking zone. In Table 2, the computed values of eroded and deposited sediment volumes are compared with the measured data. Good agreement is observed between the two except for the eroded volume from the 124th street line. The difference may be attributed to the positive net longshore sediment transport in the field. It should also be remarked that possible slow accretionary processes between pre- and post-storm profile measurement periods are not accounted for in the current numerical model.

Finally, analyzing the data used in the numerical examples, the best-fit empirical formula for λ_2 can be developed, as shown in Figure 21:

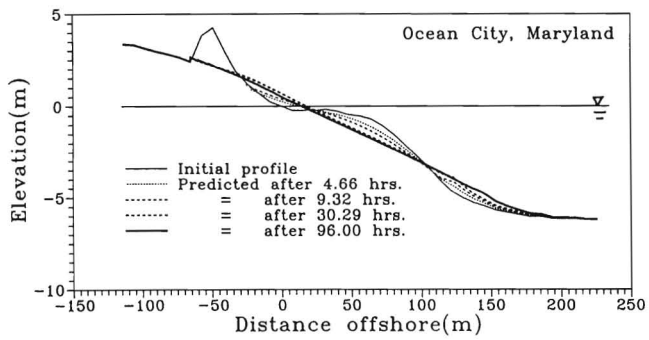

Figure 19. Time evolution of beach profile (63rd street).

Table 2. *Comparison of the present numerical results with the measured data (Ocean City, Maryland).*

	Eroded volume V_e (m³/m)		Deposited volume V_d (m³/m)		$V_e + V_d$ (m³/m)	
Street	Measured	Computed	Measured	Computed	Measured	Computed
63rd	−84.1	−90.8	82.3	86.6	−1.8	−4.2
124th	−56.1	−74.5	75.7	75.5	19.6	1.0

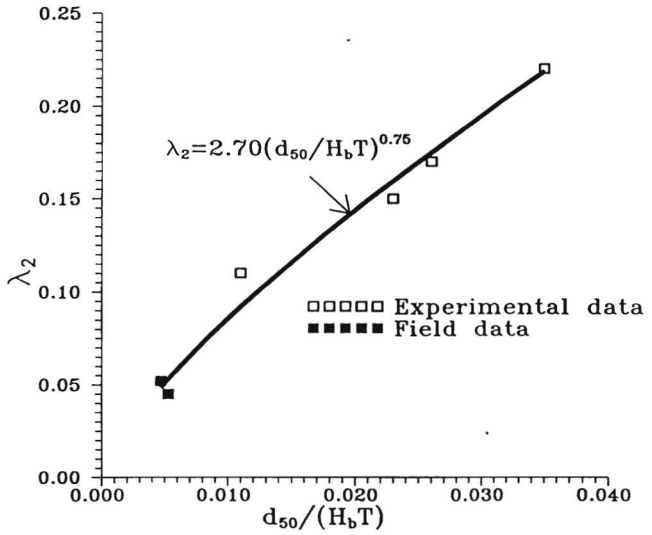

Figure 21. Least-square estimation of the parameter λ_2.

$$\lambda_2 = 2.70\left(\frac{d_{50}}{H_b T}\right)^{0.75} \tag{28}$$

in which d_{50} is the median sediment size. The units of d_{50}, H_b, and T are millimeters, meters, and seconds, respectively. We can see that the spatial decay coefficient λ_2 increases with sediment size but decreases with wave height and wave period.

CONCLUDING REMARKS

A multi-domain hybrid numerical model for the prediction of cross-shore sediment transport including bar generation and movement is developed in this paper based on the macro-scale sediment transport rate and conservation equations. The surf zone is divided into several sub-domains, and different empirically-based sediment transport rate equations are defined in each region. The solutions in each domain are matched at the patching boundaries by the continuity of the beach profile and sediment transport rate.

The hybrid numerical model reasonably simulates the erosion of beach front and dune and the growth and movement of a bar near the breaking zone. The model conserves the overall sediment volume and converges toward a steady-state solution as time becomes large. The numerical model is validated against several large-scale laboratory experiments and the field data of Ocean City, Maryland. Using the developed program, it is seen that the peak sediment transport rate does not necessarily occur at the plunging point and can be negative as time becomes large. The bar formation is shown to be sensitive to the variation of a storm surge hydrograph with time. It is also shown that the present numerical model can be extended to the multiple-bar problems. The numerical model does not include longshore sediment transport or dune and berm overwash and inundation, which need to be investigated in the future.

LITERATURE CITED

BOCZAR-KARAKIEWICZ, B.; FORBES, D.L., and DRAPEAU, G., 1995. Nearshore Bar Development in Southern Gulf of St. Lawrence, *Journal of Waterway, Port, Coastal and Ocean Engineering* (ASCE), 121(1), 49–60.

BRUUN, P., 1954. Coast Erosion and the Development of Beach Profiles, *Technical Memorandum No.* 44, Beach Erosion Board, Coastal Engineering Research Center, U.S. Army Engineer Waterway Experiment Station, Vicksburg.

DALLY, W.R. and DEAN, R.G., 1984. Suspended Sediment Transport and Beach Profile Evolution, *Journal of Waterway, Port, Coastal and Ocean Engineering* (ASCE), 110(1), pp. 15–33.

DAVIDSON-ARNOTT, R.G.D., 1981. Computer Simulation of Nearshore Bar Formation, *Earth Surface Processes and Landforms,* 6, 23–34.

DEAN, R.G., 1977. Equilibrium Beach Profiles: U.S. Atlantic and Gulf Coasts, *Technical Report No. 12,* Ocean Engineering Program, Department of Civil Engineering, University of Delaware.

DEAN, R.G., 1991. Equilibrium Beach Profiles: Characteristics and Applications, *Journal of Coastal Research,* 7(1), 53–84.

DEAN, R.G.; SRINIVAS, R., and PARCHURE, T.M., 1992. Longshore Bar Generation Mechanisms, *Proceedings of the 23rd Coastal Engineering Conference* (ASCE), pp. 2001–2014.

DETTE, H.H. and ULICZKA, K., 1987. Prototype Investigation on Time-Dependent Dune Recession and Beach Erosion, *Proceedings of Coastal Sediments '87* (ASCE), pp. 1430–1444.

KAJIMA, R.; SHIMIZU, T.; MARUYAMA, K., and SAITO, S., 1982. Experiments on Beach Profile Change with a Large Wave Flume, *Proceedings of the 18th Coastal Engineering Conference* (ASCE), pp. 1385–1404.

KEULEGAN, G.H., 1948. *An Experimental Study of Submarine Sand Bars,* Technical Report No. 3, Beach Erosion Board, Coastal Engineering Research Center, U.S. Army Engineer Waterways Experiment Station, Vicksburg, Mississippi.

KOBAYASHI, N., 1987. Analytical Solution for Dune Erosion by Storms, *Journal of Waterway, Port, Coastal and Ocean Engineering,* 113(4), 401–418.

KRIEBEL, D.L. and DEAN, R.G., 1985. Numerical Simulation of Time-Dependent Beach and Dune Erosion, *Coastal Engineering,* 9, 221–245.

LARSON, M. and KRAUS, N.C., 1989. *SBEACH: Numerical Model for Simulating Storm induced Beach Change,* Technical. Report 1, CERC-89-9, Coastal Engineering Research Center, U.S. Army Engineer Waterway Experiment Station, Vicksburg, Mississippi.

LARSON, M. and KRAUS, N.C., 1994. Temporal and Spatial Scales of Beach Profile Change, Duck, North Carolina, *Marine Geology,* 117, 75–94.

LARSON, M.; KRAUS, N.C., and BYRNES, M.R., 1990. *SBEACH: Numerical Model for Simulating Storm induced Beach Change,* Technical. Report 2, CERC-89-9, Coastal Engineering Research Center, U.S. Army Engineer Waterway Experiment Station, Vicksburg, Mississippi.

LEE, C.E.; KIM, M.H., and EDGE, B.L., 1996. Numerical Model for On-Offshore Sediment Transport with Moving Boundaries, *Journal of Waterway, Port, Coastal and Ocean Engineering,* 122(2), 84–92.

LIPPMANN, T.C. and HOLMAN, R.A., 1990. The Spatial and Temporal Variability of Sand Bar Morphology, *Journal of Geophysical Research,* 95, (C7), 11575–11590.

NAIRN, R.B., Problems Associated with Deterministic Modelling of Extreme Beach Erosion Events, *Proceedings of Coastal Sediment, 91* (ASCE), pp. 588–602.

NISHI, R. and SATO, M., 1994. Numerical Study on Beach Profile Evolution due to Random Waves, *International Symposium: Waves-Physical and Numerical Modelling,* IAHR, pp. 1530–1539.

ROELVINK, J.A. and BROKER, I., 1993. Cross-shore Profile Models, *Coastal Engineering,* 21, 163–191.

SALLENGER, A.H.; HOLMAN, R.A., and BIRKEMEIER, W.A., 1985. Storm-Induced Response of a Nearshore-Bar System, *Marine Geology,* 64, 237–257.

SMITH, E.R. and KRAUS, N.C., 1991. Laboratory study of wave

breaking over bars and artificial reefs, *Journal of Waterway, Port, Coastal and Ocean Engineering*, 117(4), 307–325.

SOUTHGATE, H.N., 1991. Beach Profile Modelling: Flume Data Comparisons and Sensitivity Tests, *Coastal Sediments '91* (ASCE) pp. 1829–1841.

STAUBLE, D.K.; GARCIA, A.W., and KRAUS, N.C., 1993. Beach nourishment project; response and design evaluation: Ocean City Maryland. Rep. 1 Technical Rep. CERC 93-13, US Army WES, Vicksburg, Mississippi.

VAN HIJUM, E., 1975. Equilibrium Profiles of Coarse Material Under Wave Attack, *Proceedings of the 14th Coastal Engineering Conference* (ASCE) pp. 939–957.

VAN HIJUM, E., 1977. Equilibrium Profiles and Longshore Transport of Coarse Material Under Oblique Wave Attack, *Proceedings of the 15th Coastal Engineering Conference* (ASCE), pp. 1258–1276.

WISE, R.A.; KOBAYASHI, N., and WURJANTO, A., 1991. Cross-Shore Sediment Transport under Irregular Waves in Surf Zones, *Coastal Sediment '91* (ASCE), pp. 658–673.

ZHENG, J. and DEAN, R.G., 1995. *Comparisons of Erosion Models for January 4, 1992, Storm at Ocean City, Maryland*, Coastal and Oceanographic Engineering Department, University of Florida.

APPENDIX—Formulation of Multi Bar Generation (4-Domain Model)

To generate double bars, the computational domain is divided into four instead of three sub-zones. The net sediment transport rate equations in each zone can then be defined as follows:

$$Q_1 = D\frac{\partial h}{\partial x} - K, \qquad -R(t) \le x \le x_{sb} \tag{29}$$

$$Q_2 = \hat{q}(t)e^{\lambda_1(x-\hat{x})^2}, \qquad x_{sb} \le x \le x_p \tag{30}$$

$$Q_3 = q_*(t)e^{-\lambda_2(x-x_*)^2}, \qquad x_p \le x \le x_b \tag{31}$$

$$Q_4 = q_b(t)e^{-\lambda_3(x-x_b)}, \qquad x_b \le x \le x_\infty \tag{32}$$

in which x_{sb} is the second breaking point of a reformed wave after initial breaking. Only limited information is available in the literature with regard to the location of subbreaking points. In the present paper, x_{sb} was determined based on the corresponding physical model result. After conducting parametric evaluation, the spreading parameters λ_1 and λ_2 are determined to be $\lambda_2 = \lambda_3^2$ and $\lambda_1 = 3\lambda_2/2$. Compared to the three-domain approach, Eq. (30) is newly introduced to generate double bars.

The matching boundary conditions between each zone are

$$h_1 = h_2 \quad \& \quad Q_1 = Q_2 + \eta\frac{dx_{sb}}{dt}, \qquad x = x_{sb} \tag{33}$$

$$h_2 = h_3 \quad \& \quad Q_2 = Q_3, \qquad x = x_p \tag{34}$$

$$h_3 = h_4 \quad \& \quad Q_3 = Q_4, \qquad x = x_b. \tag{35}$$

Then, the following equation can be derived from Eq. (33):

$$Q_{sb}\left\{\frac{2\beta\Delta x}{D} - 2\Delta t\lambda_1(x_{sb} - \hat{x})\right\}$$
$$= 2\beta\{h^n(x_{sb}) - h^n(x_{sb} - \Delta x)\} - K\frac{2\beta\Delta x}{D}$$
$$- \{h_o(x_{sb}) + S - h^n(x_{sb})\}\frac{dx_{sb}}{dt}\frac{2\beta\Delta x}{D} + S(x,t) - S(x,o) \tag{36}$$

where $Q_2|_{x=x_{sb}} = Q_{sb}$. In addition, we obtain the following equations from Eq. (34),

$$q_*(t) = \hat{q}(t)\frac{\lambda_1}{\lambda_2}\frac{x_p - \hat{x}}{x_* - x_p}e^{\lambda_1(x_p-\hat{x})^2}e^{\lambda_2(x_p-x_*)^2} \tag{37}$$

$$\hat{x} = \left(1 + \frac{\lambda_2}{\lambda_1}\right)x_p - \frac{\lambda_2}{\lambda_1}x_* \tag{38}$$

Finally, the remaining Eq. (35) yields

$$q_b(t) = \frac{2\lambda_2}{\lambda_3}q_*(t)(x_b - x_*)e^{-\lambda_2(x_b-x_*)^2} \tag{39}$$

$$x_* = x_b - \frac{\lambda_3}{2\lambda_2} \tag{40}$$

Therefore, all the unknowns in Eqs. (29)–(32) can be determined from Eqs. (36)–(40). Then, it is possible to obtain the multi-bar solution using the sediment conservation equation.

In addition, the criteria for the parameters λ_1, λ_2 and λ_3 can easily be determined from Eqs. (38) and (40)

$$x_{sb} \le \left(1 + \frac{\lambda_2}{\lambda_1}\right)x_p - \frac{\lambda_2}{\lambda_1}x_* \le x_p \tag{41}$$

$$o \le \frac{\lambda_3}{2\lambda_2} \le x_b - x_p. \tag{42}$$